INSTITUT DE FRANCE
Académie des sciences

Comptes Rendus

Géoscience

Sciences de la Planète

Milan Stafford Tchouatcha, Arnaud Patrice Kouske, Arthur Paterne Mioumnde, Amr Said Deaf and Timoleon Ngnotue

Paleoenvironmental significance and provenance of the Cretaceous calcareous deposits from the Djerem sub-basin (Adamawa, Cameroon) during the Gondwana evolution: sedimentary structures and geochemical constraints

Volume 353, issue 1 (2021), p. 265-284

Published online: 29 July 2021

https://doi.org/10.5802/crgeos.67

Les Comptes Rendus. Géoscience — Sciences de la Planète *sont membres du Centre Mersenne pour l'édition scientifique ouverte*
www.centre-mersenne.org
e-ISSN : 1778-7025

Comptes Rendus
Géoscience — Sciences de la Planète
2021, 353, nº 1, p. 265-284
https://doi.org/10.5802/crgeos.67

Original Article — Petrology, Geochemistry

Paleoenvironmental significance and provenance of the Cretaceous calcareous deposits from the Djerem sub-basin (Adamawa, Cameroon) during the Gondwana evolution: sedimentary structures and geochemical constraints

Milan Stafford Tchouatcha *, [a, b], **Arnaud Patrice Kouske** [c], **Arthur Paterne Mioumnde** [d], **Amr Said Deaf** [e] **and Timoleon Ngnotue** [a]

[a] Department of Earth Sciences, University of Dschang, P.O. Box 67, Dschang, Cameroon

[b] Higher Institute of Chemistry and Management, P.O. Box 4789, Yaoundé, Cameroon

[c] University Institute of Technology, University of Douala, P.O. Box 8698, Douala, Cameroon

[d] Institute for Geological and Mining Research, B.P. 4110, Yaoundé, Cameroon

[e] Department of Geology, Faculty of Science, Assiut University, Assiut, 71516, Egypt

E-mails: inter_milanac@yahoo.fr (M. S. Tchouatcha), arnaudpatricek@gmail.com (A. P. Kouske), arthurmioumnde@yahoo.com (A. P. Mioumnde), asdeaf75@yahoo.com (A. S. Deaf), tngnotue@yahoo.fr (T. Ngnotue)

Abstract. The calcareous deposits were affected by syn-sedimentary (lamination, bedding, convolute, ripple marks, pseudo-nodule) and post-sedimentary structure (diaclase, fault, and desiccation crack). Lamination and bedding expressed by color variation and granulometry are linked to a calm period of sedimentation and seasonal fluctuations and are periodically affected by seismic shocks giving the convolute bedding and pseudo-nodules. The presence of symmetrical ripple marks and desiccation cracks indicate respectively back and forth water movements and periodic phases of emersion characteristics of lacustrine to swampy environments. According to geochemistry data, the major element composition classifies the studied samples as shales and wackes. High LREE/HREE ratios (9.07–13.08; average: 11.77); slight positive and negative Eu anomaly (0.98–1.11); Al_2O_3/TiO_2 ratios (16.52–21.87; average: 19.73), Th/Co ratios (1.24–4.18; average: 2.26), La/Sc versus Th/Co and Zr versus TiO_2 plots indicate sediments derived from felsic rocks. The K_2O/Na_2O ratios (0.24–1.90; average: 1.01); index of compositional variability (0.88–1.35); PIA (64.94–98.42) and the Zr/Sc versus Th/Sc diagram indicate

* Corresponding author.

that the source rocks have experienced globally a moderate recycling and sorting as well as moderate weathering. The chemical index of alteration values and the SiO_2 versus $Al_2O_3 + K_2O + Na_2O$ diagram could indicate relatively warm and arid to semi-arid climate during deposition of sediments. The Sr/Ba (0.22–2.01; average: 0.58) ratios indicate a variant salinity. The Y/Ho (<40) and U/Th (<0.75) suggest respectively nonmarine environment and oxic conditions. The Djerem continental sub-basin would not have undergone marine influences yet known in the Nigeria basins of Benue.

Keywords. Calcareous deposits, Sedimentary structures, Geochemistry, Paleoenvironment, Provenance, Djerem sub-basin, Cameroon.

Manuscript received 14th September 2020, revised 9th February 2021 and 23rd May 2021, accepted 14th June 2021.

1. Introduction

Sedimentary structures and geochemistry analyses play a key role in the reconstruction of depositional conditions. The various structures observed in sedimentary rocks reflect the environmental conditions as well as the evolution of the depositional settings. These geological elements had been widely used to reconstruct the depositional environment of several sedimentary basins, including the Cretaceous sedimentary basins in Cameroon, for example, the Babouri-Figuil sedimentary basin [Ndjeng, 1992], and the Mamfe sedimentary basin [Eyong, 2003].

The Djerem continental sub-basin (Figure 1) is located along the Precambrian fault (Central Cameroon Shear Zone, CCSZ) and belongs to the basins which are linked to the South Atlantic Ocean opening occurred between the Late Jurassic and the Early Cretaceous [Ngangom, 1983]. This opening would have reactivated the old intracontinental faults causing the collapses (rifts or graben).

The Djerem sub-basin represents the western part of the southern trough of the Adamawa plateau, and the Mbere trough represents its extension eastward [Ngangom, 1983, Tchouatcha et al., 2010, 2016, Tchouatcha, 2011]. These two sub-basins contain identical basement deposits. However, the Djerem sub-basin shows some peculiarities including the presence of calcareous deposits of Cretaceous age.

Detrital terrigenous sedimentary rocks are composed of at least 50% debris from erosion of preexisting rocks. These rock types represent 80%–90% of sedimentary rocks and constitute the majority of deposit in the Djerem sub-basin [Tchouatcha, 2011]. The weathering processes yield particles of various sizes and shapes, which later on form detrital sediments. Detrital sedimentation dominates the lithologies in the Djerem sub-basin, while the chemical aspects in this deposit are represented by calcareous cement. The cement in the bottom layer contains both detrital and metamorphic parts; the later were affected by metamorphism of weak intensity [Tchouatcha, 2011].

Detrital rocks contain variable proportions of carbonates in line with the formation processes and environment of deposition. This carbonate may have a diverse origin (detrital, organic, or chemical). The nature of the cement in detrital sedimentary rocks and the physical properties of grains (nature, size, degree of wear) are precious information in the reconstitution of deposit environments.

According to Taylor and McLennan [1985], fine-grained clastic sedimentary rocks are more useful to constraint the geochemical signatures than the coarse ones. The geochemical signatures, especially that of the rare earth and trace elements, have been also widely used as proxies for the attributes of depositional settings. These geochemical signatures vary with respect to different sedimentary environments [e.g., lacustrine environment Wen et al., 2007, Chuang et al., 2016, Delu et al., 2017; mixing of river and sea waters, Hoyle et al., 1984; seawater conditions, Nothdurft et al., 2004].

Like several other continental basins of Cameroon, the geochemical data in the Djerem basin are still lacking. In fact, up to our knowledge, no geochemical study related to provenance, and sedimentation conditions have been carried out in this basin. In this paper, we will discuss the nature of source rocks of the Cretaceous fine-grained calcareous deposits in the Djerem sub-basin as well as the characteristics of weathering intensity, redox conditions, paleoclimate, and tectonic setting based on mineralogical, geochemical, and sedimentary structures analyses.

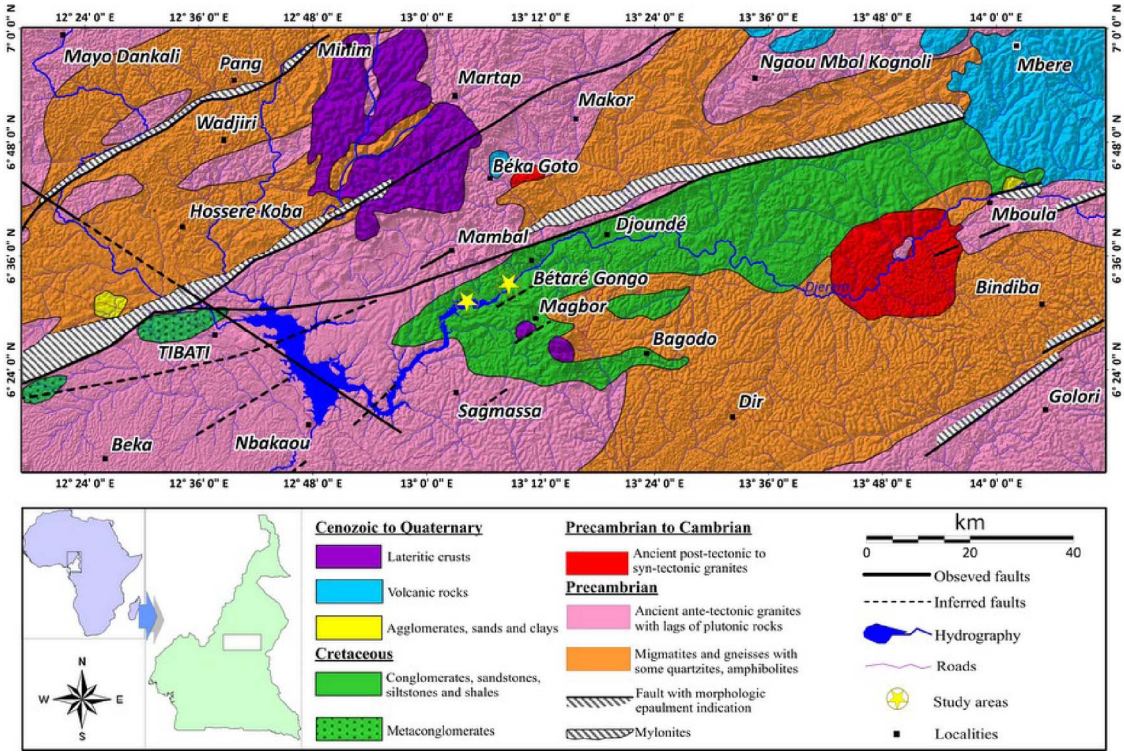

Figure 1. Geological map of the Djerem sub-basin [modified from Tchouatcha, 2011].

2. Geological setting

The study area is located in the western part of the Djerem trough that constitutes with Mbere (at the East) the same lithological unit (Figure 2) at the south of the Adamawa plateau (Djerem–Mbere). The Djerem (at the west) and the Mbere (at the east) represent two sub-basins forming a whole trough located at the South of the Adamawa plateau. They are separated by Cenozoic volcanic rocks covering that plateau. In the Mbere sub-basin, the depression is limited by two straight faults exhibiting cliffs of more than 500 m high. In the Djerem sub-basin, the external aspects of the trough are no more clearly visible because the northern margin can be only seen describing a cliff of about 300 m high, while the southern margin has been completely eroded.

The geologic evolution of the Djerem sub-basin goes in line with the general setting of the Adamawa region [Eno Belinga, 1966, 1972, Ndjeng, 1978]. The basement is constituted by metamorphic rocks (essentially migmatites, gneiss, amphibolites, and quartzites) crosscut by magmatic rocks [ante, syn and late tectonic granites, Lasserre, 1962] and both sets of rocks seem to form a united entity. This basement complex has been emplaced during several orogenic cycles in the Precambrian.

The geology of the study area, as well as of that of the Adamawa, was eroded from the Cambrian to the end of the Jurassic, and the corresponding heritage would undoubtedly be the Gondwana surface (erosional surface). It is only during the Early Cretaceous, with the dislocation of the Gondwana and opening of the South Atlantic Ocean, that the geological evolution of that area started with the filling of the southern Adamawa trough by detrital deposits whose base would be the continental infill in line with the pull-apart tectonic model [Tchouatcha, 2011].

The thickness of the Cretaceous sedimentary series in the southern Adamawa trough vary between 1600 m and 2100 m [Collignon, 1970, Noutchogwe Tatchum, 2004, Kande Houetchak, 2008, Noutchogwe Tatchum et al., 2010] and may be more important in the east [Essissima-Essissima,

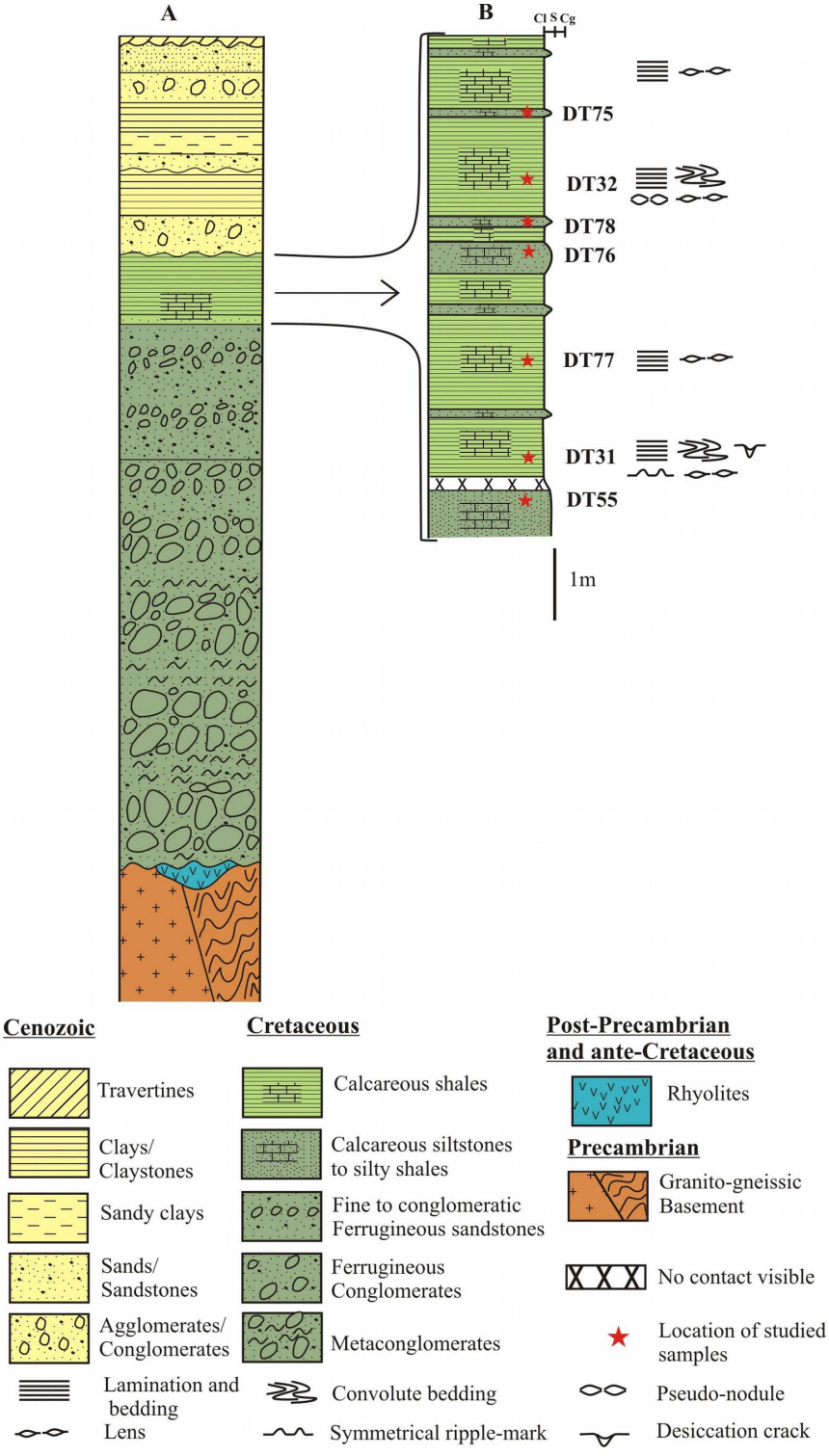

Figure 2. Synthetic log of the Djerem–Mbere basin showing the location of studied stratigraphic level [modified from Tchouatcha, 2011]. Abbreviation: Cl = clay; S = sand; Cg = conglomerate.

2001, Noutchogwe Tatchum, 2004]. They are largely dominated by conglomerates that are affected in their lower part by metamorphism of weak intensity. Meanwhile, according to Ngangom [1983], the thickness of these conglomerates may be more than 3000 m.

The metamorphic process affecting the basement conglomerates remains unknown. The regional extension of these meta-conglomerates suggests that the metamorphism process occurred after the diagenesis. In addition, the steepness of layers in contact with the basement in certain areas near adjacent faults suggests a dynamothermic metamorphism provoked by the movements of the above-mentioned adjacent faults. The late Cretaceous period in the Adamawa area was marked by a new epirogenesis [Eno Belinga, 1972] during which breakdown, subsidence, and mylonization occurred.

According to Le Maréchal and Vincent [1971], conglomerates may have been affected by thermic metamorphism of regional extension provoked by longitudinal and latitudinal fractures that were responsible for the rising up of the axial part and the subsidence of the tectonic trough. Thus, such a metamorphism may be of Pyrenean type [Ravier, 1959].

The other sedimentary rocks found in the Cretaceous series are ferruginous fine- to coarse-grained sandstones whose thickness varies between 300 and 400 m [Kande Houetchak, 2008]. The top of the series, the studied section, is constituted by calcareous facies such as calcareous siltstones and shales [Tchouatcha, 2011].

Recent studies have evidenced the presence of Cenozoic formations based on palynological data [Tchouatcha et al., 2010, Tchouatcha, 2011]. However, some deposits are hypothetically attributed to the lower Cenozoic (Eocene) based on correlations. The whole set of Cenozoic deposits are composed from bottom to top by ferruginous conglomeratic sandstones, claystones with sandy intercalations, fine- to coarse-grained ferruginous sands containing gravels, variegate clays, black clays, conglomerates with sandy clayed matrix, and white unconsolidated sandstone. These deposits are well-observed in the East.

The travertines or calcareous tuffs are more observed in the East. These deposits of Pleistocene to Holocene age have been emplaced, thanks to the movements of adjacent faults [Tchouatcha et al., 2016].

The volcanic activities are episodic and related to the tectonic movements [Eno Belinga, 1972, Tchouatcha et al., 2010]. The Upper Cretaceous is essentially characterized by the occurrences of fractures, subsidence, and volcanic activities of fissural type. These basalts are indirectly known by advance lateritic weathering processes, which have developed bauxitic plateau in the Mounts Ngaoundal and Ngaoundourou as well as in Minim and Martap areas [Eno Belinga, 1972].

Acidic volcanic events are known in the Burdigalian period during the flexuration event that affected the Adamawa plateau [Eno Belinga, 1972]. Rhyolitic outcrops are observed in the east along the southern margin of the trough where outcrops of basalts basanites and trachy-phonolite occur. The occurrence of these rock types suggests a fissural volcanic type that cross cut the basement and sedimentary formation of Cretaceous age. The basaltic cover that underlines the geographic limit between the Djerem and the Mbere sub-basins erupted from the Adamawa plateau in line with Cenozoic tectonic evolution.

3. Methods

To better understand the conditions of sedimentation of the studied deposits, field studies were carried out to describe and reconstruct all syn- and post-sedimentary structures and their relationship and chronology.

A total of 14 samples on about 7.50 m high of the stratigraphic column have been collected for geochemical, petrographic, and X-ray diffraction (XRD) analyses. Fourteen polished thin sections were prepared at Langfang Rock Detection Technology Services Ltd in Hebei (China) and in the Assiut University, Egypt. The petrographic study of these samples was carried out under the polarized microscope at the Laboratory of Petrology and Structural Geology, in the University of Yaoundé 1, Cameroon.

The X-ray diffraction patterns were obtained from a Bruker D8-Advance Eco 1 Kw diffractometer (Copper Kα radiance, λ = 1.5418 Å, V = 40,125 kV, I = 25 mA) with Lynxeye Xe energy dispersive detector in the laboratory of "Argiles, Géochimie et Environments Sédimentaires (AGES)" at the University

of Liege, Belgium. The analyses were carried out on the bulk material (nonoriented powder with grinded particles < 50 mm) of four representative samples (shales and wackes).

Whole-rock geochemical analyses of seven representative samples were carried out at Bureau Veritas Commodities, Vancouver, Canada. Prepared samples (homogenized powder) were mixed with LiBO2/Li2B4O7 flux. Crucibles were fused in a furnace at 1000 °C. The cooled bead was dissolved in ACS grade nitric acid. Trace elements (including rare earth elements (REE)) were determined by the inductively coupled plasma mass spectrometry. Major element oxides were obtained by inductively coupled plasma-atomic emission spectrometry. Loss on ignition (LOI) was determined by igniting a sample split then measuring the weight loss. The assays uncertainties varied from 0.1% to 0.04% for major elements, 0.1–0.5% for trace elements, and 0.01–0.5 ppm for REE. Accuracy for REE is estimated at 5% for concentrations >10 ppm and 10% when lower.

4. Results

4.1. *Field and sedimentary structure descriptions*

The first outcrop observed by Guiraudie [1955] under the name "fine black sandstones" is found in a point bar. These deposits form a slope of about 7 m high (Supplementary Material 1) with several tens of meters of extension. The average dip of this outcrop is 10° to the SE and is made up of bedded clays or shales containing more or less carbonate and micas. This outcrop shows greenish gray to dark color with silty sandstones intercalations of yellowish to greyish color containing more or less carbonates. This outcrop is covered by lateritic formation. The thicknesses of the clayey levels vary from millimetric to metric (generally with millimetric silty sandstone lenses) and that of the silty sandstones from millimetric to several decimetric. Many sedimentary structures are observed on this outcrop including pseudo-nodules convoluted bedding, parallel laminae, and lenticular structures sometimes bearing coal. Many faults and joints cut across the outcrop, desiccation crack, and platelet breakdown may be observed. The outcrop is tilted toward the SE.

The second outcrop is found at the Djerem–Mayel (Supplementary Material 2) confluence and appears as slab or beds of ferro-calcareous siltstones whose thickness is less than 1 m [Tchouatcha, 2011]. The dips of this outcrop vary from 10° to 12° to the NE. This rock shows a brown-gray color and reacts positively to the Hydrochloric acid. This outcrop is marked by discrete, dark discontinuous (sometimes with undulations) inframillimetric to millimetric laminations. Additionally, conjugate fractures and platelet breakdown may be observed from place to place. These laminations may underline the schistosity.

• **Pseudo-nodules.** Pseudo-nodules (Supplementary Material 1) are complete or incomplete decimetric to pluri-decimetric balls with elliptical shape. They are usually aligned as free or connected masses and alternate with the bedding or lamination.

• **Lamination and bedding.** Laminations and bedding (Supplementary Material 1) are observed over the studied outcrops; however, they appear to be well expressed on shales. These structures are underlined by a color differentiation (black, gray to yellow gray), and granulometry, which confer them an irregular evolution. Laminae appear to be millimetric to inframillimetric, and represented by gray to yellowish clayey layers, and are sometimes lenticular (Supplementary Material 2). In certain areas, organic matters (dark in color) can be found associated with yellow to gray silt lenticular intercalations, which sometimes depict sigmoid boudins. Coal laminae of lenticular shapes can be sporadically observed as well. The thickness of these beds varies from centimeter to several decimeters and is well-developed in shales and clays. The contact between different laminae is sharp; sometimes it appears eroded with poorly preserved fossil leaves. Black laminae can also be observed in ferro-calcareous silts at the Djerem–Mayel confluence. They appear to be very thin (millimetric to inframillimetric) with varied expressions (in trace, roughly, discontinued and wavy). These laminae underline the schistosity. It is worth noting that bedding is poorly developed and the outcrop is rather characterized by platelet breakdown.

• **Convolution.** Convoluted structures (Supplementary material 1) are frequently observed on shales facies. They are poorly developed on outcrop and are sporadically observed on samples. They show dimensions varying from several centimeters to decimeters. Sometimes they show double spiral.

• **Ripple marks.** The ripple marks indicate temporary emergence linked to seasonal fluctuation

water in a basin; it is also a good indicator of paleocurrents of sedimentation. They are generally symmetric, suggesting forth and back water movements. Their size or vertical extension is generally pluricentimetric. The ripple marks are more or less abundant in the intracontinental basins of Babouri-Figuil and Mayo Oulo Lere [Ndjeng and Brunet, 1998] and Mamfe [Eyong, 2003] and indicate the floodplain deposits [Eyong et al., 2019].

• **Desiccation cracks.** Desiccation cracks are present on the shales deposits with more or less interconnected cracks and generally conical shape of centimetric opening.

• **Joints and faults.** Shale outcrops are crosscut by joints and faults (Supplementary Material 2) of various orientations, with sometimes well-preserved slickenside (Supplementary Material 2). The cardinal diagrams (Supplementary Material 3) show four orientation sets including the N85–95° E, which appears to be the dominant trend followed by the N130–145° E trend and secondarily the N40–50° E and N160–170° E. It is worth noting that the N40–50° E joint set trends parallel to the shale outcrop and the marginal fault, thus suggesting an extension.

Numerous near-parallel closely spaced and steeply dipping fractures developed at low but variable angles (N65°–N75° E) on the ferro-calcareous silstones from the Djerem river. These fractures are sometimes conjugated, configuring the ferro-calcareous siltstones into numerous diamonds to irregular blocks.

4.2. *Laboratory results*

4.2.1. *Petrography analyses*

The studied samples are subdivided into two groups according, on one hand the calcareous clayey to silty clay facies (DT31, DT32, and DT77); and on other hand the calcareous siltstones (DT55, DT75, DT76, and DT78).

• **The clayey to silty clay facies.** The clayey facies are composed of micro-grains of quartz, feldspar, micas, epidote, oxides, and a clay-carbonated binder with organic matter. Quartz (20–30%) is generally monocrystalline, and very angular to angular, rarely subangular. Feldspar (20–25%) is represented by plagioclase, orthoclase and rarely microcline, and is very angular to angular and rarely subangular. Mica is represented by needles of biotite (5–15%) and muscovite (2–4%). These minerals underline the schistosity. Epidote is very rare (<1%) and is represented by pistachite and very rarely zoisite. The oxides have rounded to subangular forms, with a proportion of about 2–3%. The binder (25–35%) is indistinguishable clay-carbonate and associated with organic matter. There are sometimes the thin intercalations of calcite (Supplementary Material 4) and coal (Supplementary Material 4) veins. Their microstructures are very fine clastic, sub-iso to isogranular (Supplementary Material 4). These shales are moderate to well-sorted.

• **The siltstones to very fine sandstones.** Siltstones to very fine sandstones are composed of quartz, feldspar, mica, epidote, oxide, and a binder of varied nature. Quartz (35–40%) is essentially monocrystalline, very angular to angular, with rare subangular to rounded grains, sometimes striated and cracked. Feldspar (30–35%) is represented by orthoclase and plagioclase, associated with rare microclines. They are generally very angular to angular, rarely subangular to rounded, sometimes cracked and kinked, and sometimes very altered (sericitization and vacuolization) (Supplementary Material 4). Mica is represented by chlorite (5–15%), muscovite (2–5%). Mica occurs either as flakes or fine needles, sometimes flexible (Supplementary Material 4) in inter-granular contact between quartz and feldspar. Chlorite generally comes from the alteration of biotite, which sometimes shows a shredded and oxidized appearance. Oxides (5–15%) are abundant in more ferruginous facies and in small proportion in more calcareous facies, and generally result from the alteration of ferromagnesians (e.g., biotite, amphibole). Epidote (<1%) is rare and usually found in single grains represented by the pistachite. The binder (5–10%) is ferruginous, calcareous (Supplementary Material 4) and siliceous (Supplementary Material 4). Their microstructure is fine clastic, sub-iso to isogranular. They are moderately sorted to well sorted.

4.2.2. *X-ray diffraction*

The X-ray diffraction analysis (Figure 3) reveals a similarity of mineralogical composition between the two groups, dominated by non-clays mineral such as quartz (dominant) and feldspars, and secondarily by clay minerals made up in descending order of chlorite, kaolinite, and illite. The chlorite and kaolinite are more abundant in the clay facies. The samples

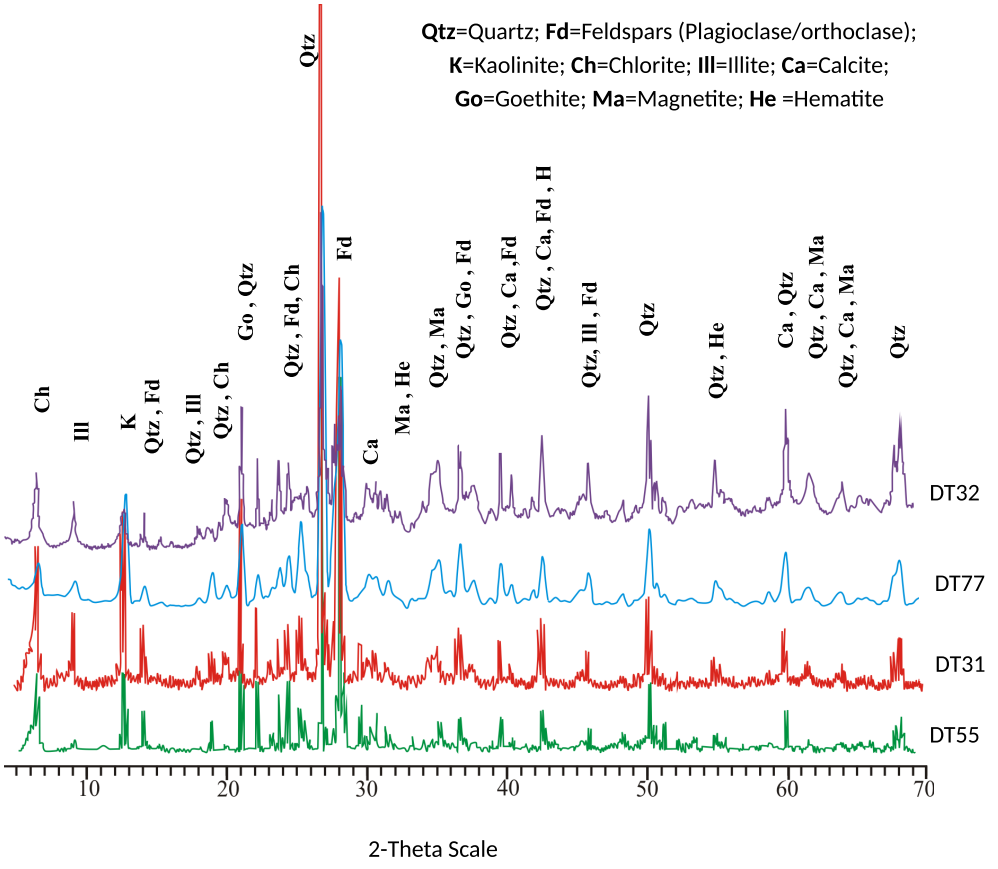

Figure 3. X-ray diffractions of representative studied samples.

are very poor in smectite and contain relatively few quantity of calcite.

4.2.3. *Geochemical data*

• **Major elements.** The SiO_2/Al_2O_3 versus FeO_3/K_2O discriminant diagram (Figure 4) of Herron [1988] shows that the studied samples are composed by shale (DT31 and DT32), Fe-shale (DT55), and wacke (DT75, DT76, DT77, and DT78).

According to Supplementary Material 5, SiO_2 and Al_2O_3 are the two abundant elements and their proportion varies from 59.92 to 71.53% and 13.13 to 17.28%, respectively. The SiO_2 concentration is high in wacke samples and low in shale samples in contrary with the Al_2O_3.

The concentrations of K_2O (1.23–4.3%) and Na_2O (2.28–5.17%) are relatively high indicating the relative abundance of potassium-bearing minerals [Moradi et al., 2016] and sodium-bearing minerals [Ross and

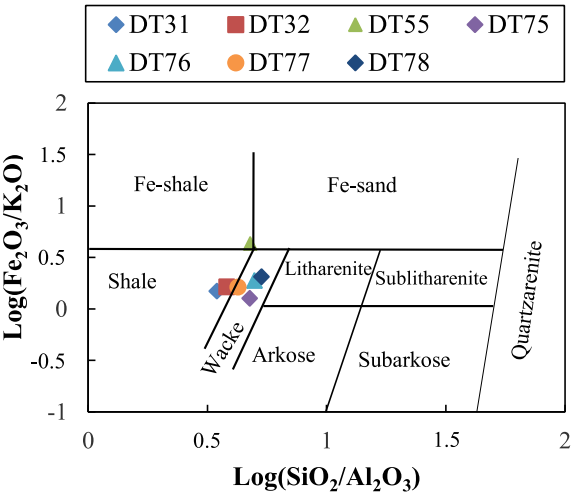

Figure 4. Classification of studied sediments according to the scheme of Herron [1988].

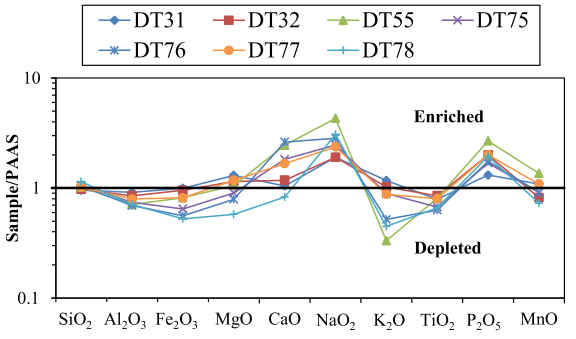

Figure 5. Major elements variations for studied sediments. Data are average values normalized to PAAS [after Taylor and McLennan, 1985 and McLennan, 2001].

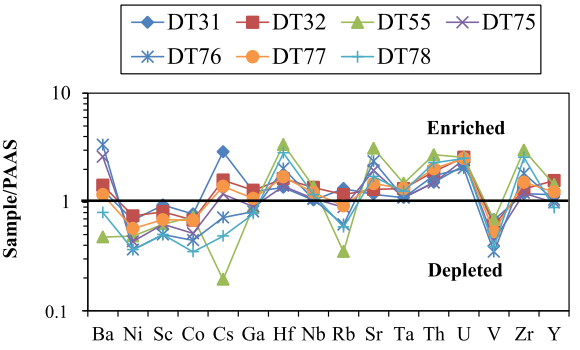

Figure 6. Trace elements variation for studied sediments. Data are average values normalized to PAAS [after Taylor and McLennan, 1985 and McLennan, 2001].

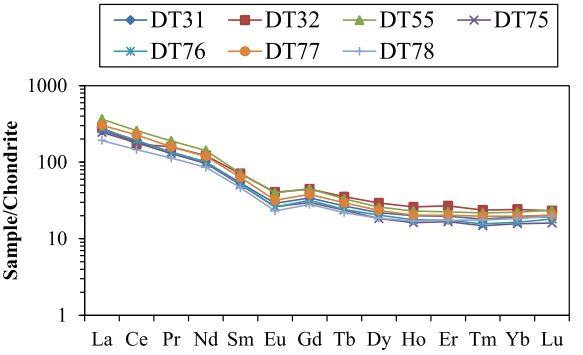

Figure 7. REE pattern for studied sediments. Data are average values normalized to chondrite [after McDonough and Sun, 1995].

Bustin, 2009] in the studied materials, but dominated by the sodium-bearing minerals. According to Supplementary Material 6, the strong positive relationships of K_2O with Al_2O_3 ($R = 0.89$) can reflect close relationship with clay and feldspar [Fu et al., 2011, Moradi et al., 2016], and relative strong negative relationship of Na_2O and Al_2O_3 ($R = -0.75$) can probably indicate a partial chemical origin of Na. The strong positive correlation between Fe_2O_3 and TiO_2 ($R = 0.91$) and Fe_2O_3 and MgO ($R = 0.94$) gives indication that they are derived respectively from same detrital mineral ilmenite and amphibole. The slight positive correlation between CaO and LOI ($R = 0.41$) and slight negative relationship between Al_2O_3 and CaO ($R = -0.5$) indicates that Ca is present in both calcite and plagioclase, but more is abundant in calcite. The Fe_2O_3 concentration in the studied materials varies from 3.41 to 6.44 due to the Fe-bearing minerals.

According to Figure 5, all the studied materials, compared to post achean Australian shales (PAAS) respectively, are enriched in P_2O_5, enriched and vary in Na_2O, vary and depleted in Fe_2O_3, depleted and vary in Al_2O_3, deplete and enriched in TiO_2, and vary in the remaining elements.

• **Trace elements.** The trace elements contents of studied samples are listed in Supplementary Material 7. Ba, Rb, Sr, and Zr are the most abundant elements, where values are varying from 309 to 2177 ppm, 55.9–212.1 ppm, 235.1–622.1, and 249.4–629.5 ppm, respectively.

According to Figure 6, all the studied materials, compared to PAAS, are enriched in Hf, Nb, Ta, Th, U, and Zr, depleted in Ni and V, depleted and vary in Sc, depleted and vary in Co, enriched and vary in Sr, vary and enriched in Y, and the contents of the remaining elements generally vary.

• **Rare Earth elements.** The contents of REE and their concentrations are listed in Supplementary Material 7. The LREE/HREE ratios range from 9.07 to 13.08 (average: 11.77), suggest an enrichment in LREE. REE concentration normalized to PAAS [Taylor and McLennan, 1985, McLennan, 2001] indicates slight positive to very slight negative Eu anomalies (Eu/Eu^* vary from 0.98 to 1.11), and negative to very slight negative Ce anomalies (Ce/Ce^* vary from 0.77 to 0.98).

For comparison, REE composition of the studied samples and the PAAS were normalized to the chondrite [McDonough and Sun, 1995; Figure 7]. The

chondrite-normalized REE pattern confirms broadly the similar LREE-enrichment for the studied samples and the slight negative Eu anomalies for all samples.

Usually, when having the same origin, Eu and Ce anomalies as well as the REE patterns of the sediments are similar [Zeng et al., 2019]. Based on the chondrite-normalized REEs (Figure 11), the studied samples show the similar REE patterns indicating both REE and Eu mainly inherited from parent rocks.

5. Discussion

5.1. *Mechanisms of sedimentation*

Basal calcareous deposit of the study section is probably of early Cretaceous age and has been interpreted either as has being derived from distal fluviatile origin, fluvial current, or lower energy fluviolacustrine deposits [Tchouatcha, 2011]. This formation may be linked to the transtensional phase that provoked the modification of the trough in the south of Adamawa. Calcitic cement (probably of primary nature) and ferruginous cement, as well as the fine texture of silts, suggest an open shallow deep lacustrine environment, favorable to the proliferation of an algo-microbial population and the supply by fine detrital and distal matters.

The Cretaceous sequence is covered by bedded clayed deposits or calcareous shales marked by silty sandstones and coal intercalations. According to Guiraudie [1955], the deposits of the studied section may correspond to the Wealdian facies. However, recent studies situated them in the middle Cretaceous, probably Albian to Cenomanian based on correlations with those of the Mamfe sub-basin located in the west [Eyong, 2003, Njoh et al., 2015]. These materials represent infilling clogging deposits and may correspond to a swampy sedimentation following a blockage, which may have occurred in the east, but destructive strengths being more or less active in the west (Djerem) provoking lifting-up and collapse in the area. Sedimentation took place by periodic influx of fine to very fine detrital materials in anoxic conditions. This sedimentation was periodically influenced by the seismic waves [Cojan and Thiry, 1992] provoked by syn- to post-tectonic movements by activities of marginal faults as suggested by the presence of sedimentary structures such as convolute and pseudo-nodules (syn-sedimentary) associated to fault and joints (post-sedimentary). All hypotheses leading to convolute lamination require unconsolidated sediment during deformation [Gladstone et al., 2018]. These structures are generally associated with turbiditic sequences, but they can be very abundant in sediments in intertidal zones as well as in fluvial environments [Freidman and Sanders, 1978, Reineck and Singh, 1980]. In addition, laminations and bedding suggest a calm depositional environment; however, with variable velocity. The occurrence of laminations suggests a high velocity, while bedding rather suggests a lower velocity with respect to quantity of detrital materials, the latter was influenced by the climate type. The alternation of laminations or bedding with levels of pseudo-nodules suggests an alternation of calm and more agitated periods caused by the tectonic activity. The presence of organic matter as well as coal-rich silty sandstones may suggest fluctuating water table (repeated flood and land emerge), which characterizes wet lands. This deposit indicates a hot and dry climate. Calcitic cement may be of primary nature linked to a periodically shallow deep environment favorable to the proliferation of algomicrobic and thus diagenetic alterations.

5.2. *Provenance*

5.2.1. *Source lithotype*

For source lithotype, many plots have been proposed and widely used such as Th/Co versus La/Sc [Cullers, 2002, Ngueutchoua et al., 2017] and Zr versus TiO_2 [Hayashi et al., 1997, Ngueutchoua et al., 2019]. The location of the studied materials on these scattered plots shows that the geochemical signatures of the source lithotype correspond to felsic rocks (Figure 8(A)) and silicic rocks (Figure 8(B)).

Many ratios have been also used to characterize the source rocks such as Th/Co ratio [Cox et al., 1995, Cullers, 2000, Armstrong-Altrin et al., 2015, Tawfik et al., 2017] and Al_2O_3/TiO_2 ratio [Hayashi et al., 1997, Daï et al., 2011, Ma et al., 2015, Zeng et al., 2019]. In our studied materials, the Th/Co ratios vary from 1.24 to 4.18 (average 2.26). These ratios vary from 0.67 to 19.4 in the felsic source and from 0.04 to 1.10 in the mafic source, indicating essentially the felsic source rocks of our sediment with negligible contribution of mafic rocks. The Al_2O_3/TiO_2 ratio is generally greater than 21 in felsic source rocks, 8–21 in intermediate

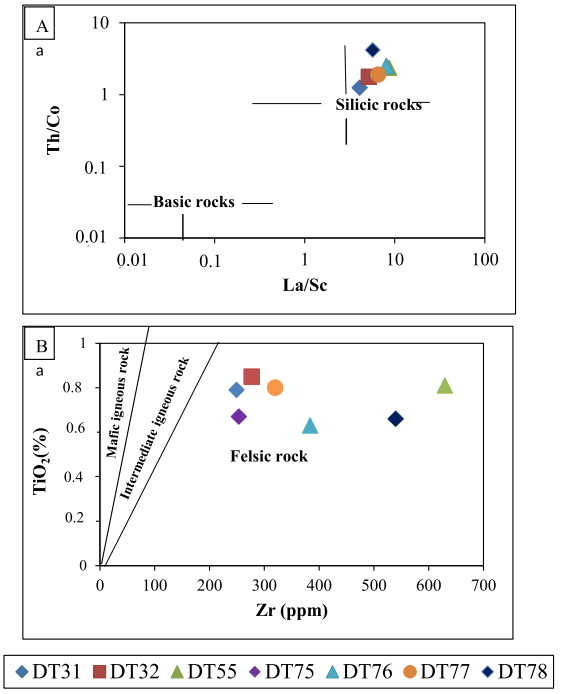

Figure 8. Scatter plots of (A) Th/Co versus La/Sc [Cullers, 2002] and (B) TiO_2 versus Zr, showing nature of the studied samples.

rocks and less than 8 in mafic source rocks. This ratio ranges from 16.32 to 21.87 (average: 19.73) suggesting essentially a felsic source rock.

The REE patterns and size of Eu anomaly have been used to characterize the mother rocks of sediments [Taylor and McLennan, 1985, Armstrong-Altrin et al., 2014, Liu et al., 2015, Ma et al., 2015, Zeng et al., 2019]. Felsic rocks contain higher LREE/HREE ratios and negative Eu anomaly, and mafic rocks usually contain low LREE/HREE ratios and little or no negative Eu anomaly [Armstrong-Altrin et al., 2014].

The LREE/HREE ratios range from 9.07 to 13.08 (average: 11.77). The Eu anomaly values, range from 0.98 to 1.11, are indicative of essentially felsic provenance as all the LREE/HREE values of our studied materials are lower to the PAAS (13.18).

5.2.2. *Sediments sorting and recycling and paleoweathering*

Many ratios have been used to indicate chemical maturity of some deposits such as K_2O/Na_2O [Mongelli, 2004, Ngueutchoua et al., 2017]. This ratio increases with weathering due to more liable nature of plagioclase relative to K-feldspar [Nesbitt and Young, 1982]. A ratios > 1, indicate high chemical maturity [Armstrong-Altrin et al., 2016]. In this study, the K_2O/Na_2O ratio vary from 0.24 to 1.90, suggesting globally a moderate amount of sediment recycling.

In addition, other parameters such as chemical index of alteration (CIA) and index of compositional variability (ICV) have been used to characterize the compositional maturity of sediments [e.g., Mongelli et al., 2006, Perri et al., 2011, Tao et al., 2013, Perri, 2014, Absar and Sreenivas, 2015, Armstrong-Altrin et al., 2015, Ngueutchoua et al., 2017, Tawfik et al., 2017]. ICV > 1 indicates immature sediments and ICV < 1 shows mature sediments. The ICV values of the studied sediments range from 0.88 to 1.35 (average 1.11) higher than the PAAS (0.84) indicating the submature characters of sediments. High values of CIA (76–100) indicate intense chemical weathering, whereas low values (CIA ≤ 50 reflect unweathered source areas. The CIA values vary from 58.25 to 68.41 (average 64.08) indicating the moderate weathered source rocks. Meanwhile, the presence of illite and K-feldspar, according to the mineralogical composition (Figure 3), may indicate a K-addition, and it is noteworthy that the CIA value may be decreased due to K-metasomatism [Fedo et al., 1995].

Furthermore, high ΣREE contents reflects a possible control by differing amounts of accessory minerals such as zircon and/or quartz linked to the recycling processes [Zou et al., 2016]. In our studied materials, ΣREE values range from 210.99 to 366.24 ppm (average: 280.31 ppm) higher than the PAAS (184.77 ppm) and UCC (146.37 ppm), indicating the recycling of these sediments.

The Zr/Sc and Th/Sc ratios are also useful parameters to depict changes in heavy mineral enrichment, sorting level, and sediment composition [McLennan et al., 1993]. High Zr/Sc ratios indicate zircon accumulation by sediment recycling and sorting. The Zr/Sc values range from 16.63 to 67.48 (average 38.67) and compared to PAAS (13.13) and UCC (13.97) indicate a moderate to high sorting and recycling of the rock provenance as confirmed by the Zr/Sc versus Th/Sc diagram (Figure 9).

The SiO_2/Al_2O_3 ratio has been also used for textural maturity of sediments [Etemad-Saeed et al., 2011, Armstrong-Altrin and Machain-Castillo, 2016, Tawfik et al., 2017]. The average SiO_2/Al_2O_3 ratio is 3 in

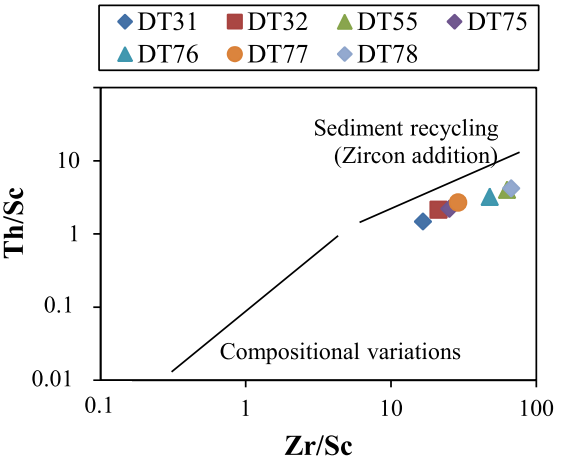

Figure 9. Th/Sc versus Zr/Sc plot of studied sediments.

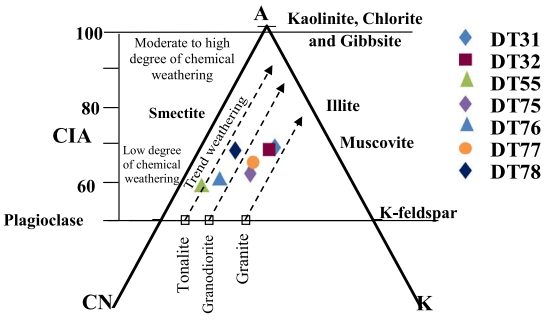

Figure 10. A–CN–K plots of Nesbitt and Young [1984] for studied samples. The dotted line represents the possible weathering trend of the source rock if no K-addition is involved. The heavy solid line represents possible weathering trend combined with K-metasomatism from the source rock.

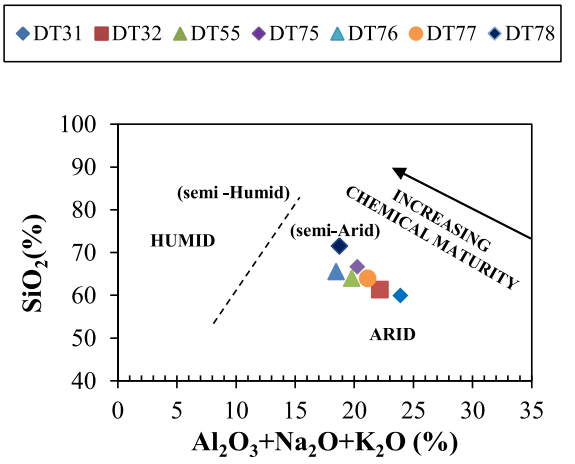

Figure 11. Chemical maturity and climate during the deposition of the studied samples expressed by bivariate plot of SiO_2 versus Al_2O_3 + K_2O + Na_2O [after Suttner and Dutta, 1986].

basic igneous rocks and about 5 in acidic igneous rocks, whereas the value > 5 in clastic sediments shows high sediment maturity [Roser et al., 1996]. The SiO_2/Al_2O_3 ratios of the studied materials range from 3.41 to 5.34 (average: 4.49) and thus characteristic of submature to mature sediments.

The CIA [Nesbitt and Young, 1982] and plagioclase index of alteration (PIA) of Fedo et al. [1995] have been widely used to infer chemical weathering of sediments [e.g., Armstrong-Altrin et al., 2015, Rashid et al., 2015, Tawfik et al., 2017, Ngueutchoua et al., 2019]. Very high PIA and CIA values (>75) indicate intense chemical weathering, whereas values ≤50 reflect little or unweathered source rocks. The PIA and CIA values range respectively from 64.94 to 98.42 (average 81.23) and 58.25–68.41 (average 64.08) indicating that the source rocks show moderate to intense chemical weathering. The A–CN–K ternary diagram of Nesbitt and Young [1984] (Figure 10) indicates that the studied sediments have mainly a mixed granite and granodiorite composition as source rocks and have probably experienced moderate to intense chemical weathering.

5.3. *Paleoclimate, paleosalinity, and paleo-oxidation conditions*

5.3.1. *Paleoclimate*

The degree of chemical weathering is function of temperature [Meunier et al., 2013] and the relationship between climate and degree of chemical weathering were established [White and Blum, 1995]. The CIA has been also used for paleoclimate indication [e.g., Nesbitt and Young, 1982, Yan et al., 2010, Zeng et al., 2019]. The climate is cold and dry during low chemical weathering if the CIA values range from 50 to 65, CIA range from 65 to 85 indicates a warm and humid climate during moderate chemical weathering and range between 85 and 100 indicates a hot and

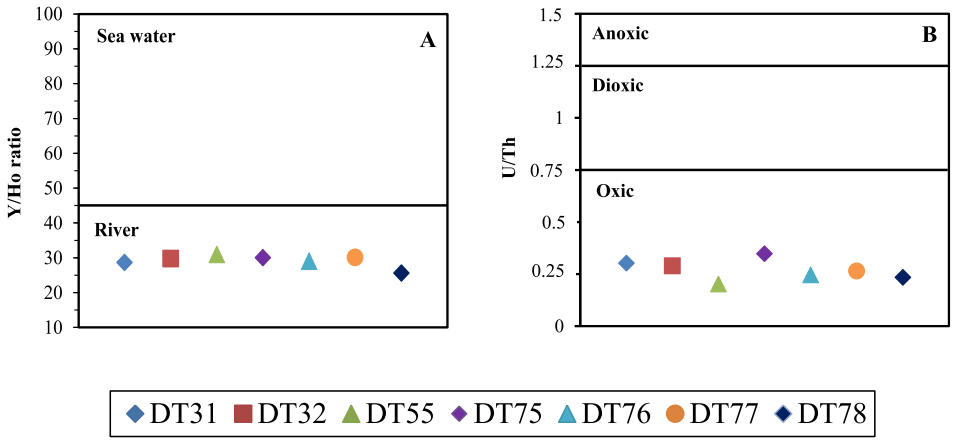

Figure 12. Plot diagrams to distinguish terrestrial and sea water (A) and depositional conditions (oxic, dioxic and anoxic conditions) (B).

humid climate during high chemical weathering. The CIA values range between 58.25 and 68.41 (average 64.08), suggest a relative warm and humid climate during moderated chemical weathering. By another way, the SiO_2 versus $Al_2O_3 + K_2O + Na_2O$ diagram of Suttner and Dutta [1986] (Figure 11) applied to the studied materials indicates an arid to semi-arid climate. Probably, the climate was relatively warm and arid to semi-arid during the deposition of the studied sediments.

5.3.2. *Paleosalinity and paleo-oxidation conditions*

For paleosalinity condition reconstruction, the Sr/Ba ratio has been widely used [e.g., Zheng and Liu, 1999, Xu et al., 2011, Cao et al., 2012, Meng et al., 2012, Ngueutchoua et al., 2019]. This ratio increases from coastal fresh water to the open and saline water [Cao et al., 2012], <1 in fresh water and >1 in marine sediments [Jones and Manning, 1994, Shi et al., 1994, Wang et al., 2005]. This ratio ranges from 0.23 to 2.01 (average 0.58) indicates according to the stratigraphic succession of samples, a hypersaline condition at the bottom (DT55 = 2.01) and fresh water condition in the upper part with more or less fluctuation (0.22–0.66).

The Y/Ho ratio is used to differentiate between continental (nonmarine) and marine environments. The Y/Ho ratio between 40 and 90 corresponds to a sea environment while Y/Ho ratio < 40 indicates a river environment [Bau and Dulski, 1996, Nozaki et al., 1997, Bolhar et al., 2004, Abigail et al., 2010, Bokanda et al., 2019]. The Y/Ho ratio ranges from 25.50 to 30.95 (average 29.10) (Figure 12(A)), suggesting river conditions.

Several ratios such as U/Th ratios have been used to better understand depositional environmental conditions [e.g., Jones and Manning, 1994, Rimmer, 2004, Teng et al., 2005, Tribovillard et al., 2006, Nagarajan et al., 2007, Zhao et al., 2016, Delu et al., 2017, Xie et al., 2018, Bokanda et al., 2019]. The U/Th ratio < 0.75, between 0.75 and 1.25 and >1.25 correspond respectively to oxic, suboxic, and anoxic conditions. All the studied samples correspond to oxic environments (Figure 12(B)).

5.4. *Tectonic setting*

To characterize the tectonic setting, of our studied sediments, we used the multidimensional diagram based on major elements of Verma and Armstrong-Altrin [2013]. This diagram is widely used in studying tectonic regimes of recent and ancient sediments [e.g., Guadagnin et al., 2015, Nagarajan et al., 2015, Zaid, 2015, Armstrong-Altrin and Machain-Castillo, 2016, Tawfik et al., 2017, Zeng et al., 2019]. This diagram shows discrimination of island or continental arc, continental rift, and collision tectonic setting from high silica ($(SiO_2)_{adj}$ = 63–95%), and low silica ($(SiO_2)_{adj}$ = 35–63%). All the studied materials belong to the high-silica group. The samples plotted (Figure 13(A)) fall in the collisional field boundary. We

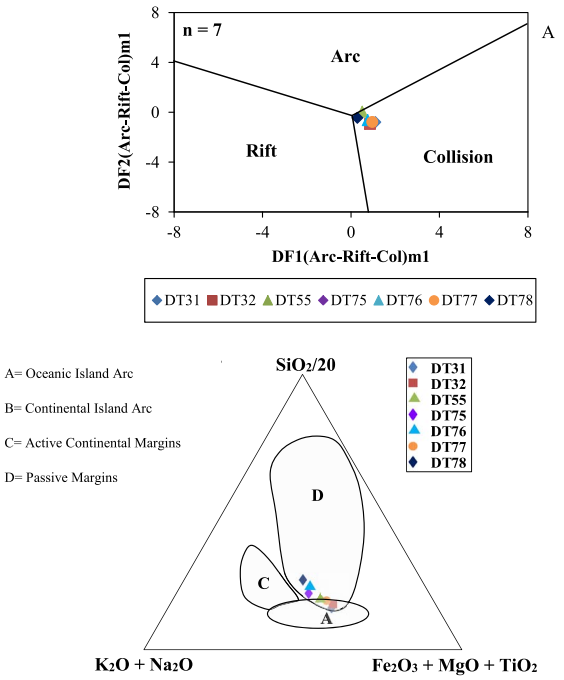

Figure 13. (A) Discriminant-function multidimensional diagram for high-silica clastic sediments [after Verma and Armstrong-Altrin, 2013]. The subscript m_1 in DF1 and DF2 represents the high-silica diagram based on $\log_e$-ratios of major elements. The discriminant-function equations are $\mathrm{DF1(Arc\text{-}Rift\text{-}Col)m_1} = (-0.263 \times \ln(TiO_2/SiO_2))_{adj} + (0.604 \times \ln(Al_2O_3/SiO_2))_{adj} + (-1.725 \times \ln(Fe_2O_{3t}/SiO_2))_{adj} + (0.660 \times \ln(MnO/SiO_2))_{adj} + (2.191 \times \ln(MgO/SiO_2))_{adj} + (0.144 \times \ln(CaO/SiO_2))_{adj} + (-1.304 \times \ln(Na_2O/SiO_2))_{adj} + (0.054 \times \ln(K_2O/SiO_2))_{adj} + (-0.330 \times \ln(P_2O_5/SiO_2))_{adj} + 1.588$. $\mathrm{DF2(Arc\text{-}Rift\text{-}Col)m_1} = (-1.196 \times \ln(TiO_2/SiO_2))_{adj} + (1.604 \times \ln(Al_2O_3/SiO_2))_{adj} + (0.303 \times \ln(Fe_2O_{3t}/SiO_2))_{adj} + (0.436 \times \ln(MnO/SiO_2))_{adj} + (0.838 \times \ln(MgO/SiO_2))_{adj} + (-0.407 \times \ln(CaO/SiO_2))_{adj} + (1.021 \times \ln(Na_2O/SiO_2))_{adj} + (-1.706 \times \ln(K_2O/SiO_2))_{adj} + (-0.126 \times \ln(P_2O_5/SiO_2))_{adj} - 1.068$. (B) Plot of the major elements composition of the stream sediments on the tectonic setting discrimination diagram of Kroonenberg [1994]. A: oceanic island arc, B: continental island arc, C: active continental margin, D: passive margin.

also used the tectonic setting discrimination ternary diagram ($SiO_2/20 - K_2O + Na_2O - Fe_2O_3 + MgO + TiO_2$) of Kroonenberg [1994]. This diagram discriminates sediments deposited in the passive continental margins (PCM), active continental margins, oceanic island arc, and continental island arc (CIA). Our plotted samples fall in the passive margins (PM) and the intersection between the PM and CIA domains (Figure 13(B)), reflecting the compressional condition. The results from these two diagrams are inconsistent with the geological setting of the studied area and could indicate the Precambrian basement history of the studied area from which are derived these deposits as the tectonic setting of source rocks may be inferred from recent sedimentary rocks [Armstrong-Altrin et al., 2015]. The Precambrian basement of the studied area belongs to Pan-African north-equatorial fold belt, which resulted from the neoproterozoic orogeny [Nzenti et al., 1988]. This orogeny recycled partially or totally the older crust materials (paleoproterozoic and archean crustal material) during collision between Congo and West African cratons and the closure of large proterozoic ocean realms [Nzenti et al., 1988, Penaye et al., 1993, Kröner and Stern, 2004, Toteu et al., 2004]. Indeed, according to the tectono-stratigraphic evolution of the Djerem–Mbere basin [Ngangom, 1983, Tchouatcha, 2011], the studied deposits correspond mainly to the extensional phase of deformation.

6. Conclusion

(1) According to the major elements composition, the studied Cretaceous calcareous deposits of the Djerem sub-basin are essentially composed of shales and wackes with subordinate Fe-shales.

(2) The observed lamination and bedding suggests that the studied sediments have been deposited globally in a calm environment marked by seasonal fluctuation and periodically affected by the seismic shocks causing the convolute bedding and pseudo-nodules, and post-diagenesis seismic lead to joints and faults. The milieu of deposition was marked by periodic emersion and forth and water giving desiccation cracks and symmetrical ripple marks, respectively.

(3) The K_2O/Na_2O ratios, the CIA and PIA values, the Zr/Sc versus Th/Sc diagram suggest that the sediments are submature to mature; the Al_2O_3/TiO_2 and Th/Co ratios and the La/Sc versus Th/Co and Zr versus TiO_2 plots indicate that the sediments are essentially derived from felsic rocks.

(4) The CIA values and the SiO_2 versus Al_2O_3 + K_2O + Na_2O diagram indicate a relative warm and arid to semi-arid climate during deposition of sediments in a swampy environment. Paleosalinity range from hypersaline at the bottom to fresh water at the top according to the Sr/Ba ratios. Oxic conditions according were prevailing to the U/Th ratios.

(5) The tectonic setting, collisional environment, or PM correspond rather to the Precambrian history that affected the basement from which are derived the studied carbonate deposits according to the discriminant function-based multidimensional and major elements composition diagrams.

Acknowledgments

The authors greatly acknowledge Dr. Sidonie Révillon for reviewing and improving the manuscript, and Dr. Mache, Local Materials Promotion Authority Cameroon, for providing mineralogical analysis facilities.

Supplementary data

Supporting information for this article is available on the journal's website under https://doi.org/10.5802/crgeos.67 or from the author.

References

Abigail, C. A., Balz, S. K., Malcolm, R. W., Ian, W., and Isik, K. (2010). Trace elements record depositional history of an early Archean stromatolitic carbonate platform. *Chem. Geol.*, 270, 148–163.

Absar, N. and Sreenivas, B. (2015). Petrology and geochemistry of greywackes of the ~1.6 Ga middle Aravalli supergroup, northwest India: evidence for active margin processes. *Int. Geol. Rev.*, 57, 134–158.

Armstrong-Altrin, J. S., Lee, Y. I., Kasper-Zubillaga, J. J., and Trejo-Ramírez, E. (2016). Mineralogy and geochemistry of sand along the Manzanillo and El Carrizal beach areas, southern Mexico: implications for palaeoweathering, provenance and tectonic setting. *Geol. J.*, 52, 559–582.

Armstrong-Altrin, J. S. and Machain-Castillo, M. L. (2016). Mineralogy, geochemistry, and radiocarbon ages of deep sea sediments from the Gulf of Mexico, Mexico. *J. South Amer. Earth Sci.*, 71, 182–200.

Armstrong-Altrin, J. S., Nagarajan, R., Balaram, V., and Natalhy-Pineda, O. (2015). Petrography and geochemistry of sand from the Chachalacas and Veracruz beach areas, western Gulf of Mexico, Mexico: constraints on provenance and tectonic setting. *J. South Amer. Earth Sci.*, 64, 199–216.

Armstrong-Altrin, J. S., Nagarajan, R., Lee, Y. I., and Córdoba-Saldaña, L. P. (2014). Geochemistry of sands along the san Nicolás and san Carlos beaches, Gulf of California, Mexico: implication for provenance. *Turkish J. Earth Sci.*, 23, 533–558.

Bau, M. and Dulski, P. (1996). Distribution of yttrium and rare-earth elements in the penge and kuruman iron-formations, transvaal 496 supergroup, South Africa. *Precambrian Res.*, 79, 37–55.

Bokanda, E. E., Fralick, P., Ekomane, E., Njilah, I. K., Bisse, S. B., Akono, D. F., and Ekoa Bessa, A. Z. (2019). Geochemical characteristics of shales in the Mamfe basin, south west Cameroon: implication for depositional environments and oxidation conditions. *J. African Earth Sci.*, 149, 131–142.

Bolhar, R., Kamber, B. S., Moorbath, S., Fedo, C. M., and Whitehouse, M. J. (2004). Characterisation of early Archaean chemical sediments by trace element signatures. *Earth Planet Sci. Lett.*, 222(1), 43–60.

Cao, J., Wu, M., Chen, Y., Hu, K., Bian, L. Z., Wang, L. G., and Zhang, Y. (2012). Trace and rare earth element geochemistry of Jurassic mudstones in the northern Qaidam basin, northwest China. *Chem. Erde*, 72, 245–252.

Chuang, E., Yangyang, L., Jingzhou, Z., Rui, W., and Zhikun, W. (2016). Characteristics of lacustrine organic-rich shale: a case study of the chang 7 member, Triassic Yanchang formation, Ordos basin, China. *J. Nat. Gas Geosci.*, 1, 173–185.

Cojan, I. and Thiry, M. (1992). Seismically induced deformation structures in oligocene shallow-marine and aeolian coastal sands. *Tectonophysics*,

206, 79–89.

Collignon, F. (1970). Rapport sur quelques profils gravimétriques et magnétiques dans la vallée de la Mbere. Rapport multigr. Centre ORSTOM, Bangui.

Cox, R., Low, D. R., and Culler, R. L. (1995). The influence of sediment recycling and basement composition on evolution of mudrock chemistry in the southwestern United States. *Geochem. Cosmochim. Acta*, 59, 2919–2940.

Cullers, R. L. (2000). The geochemistry of shales, siltstones, and sandstones of Pennsylvanian–Permian age, Colorado, USA: implications for provenance and metamorphic studies. *Lithos*, 51, 181–203.

Cullers, R. L. (2002). Implications of elemental concentrations for provenance, redox conditions, and metamorphic studies of shales and limestones near Pueblo, CO, USA. *Chem. Geol.*, 191, 305–327.

Daï, S., Wang, X., Zhou, Y., Hower, J. C., Li, D., Chen, W., and Zou, J. (2011). Chemical and mineralogical compositions of silicic, mafic, and alkali tonsteins in the late Permian coals from the Songzao coalfield, Chongqing, southwest China. *Chem. Geol.*, 282, 29–44.

Delu, L., Rongxi, L., Zengwu, Z., Xiaoli, W., Futian, L., Bangsheng, Z., Jinghua, C., and Baoping, W. (2017). Elemental characteristics and paleoenvironment reconstruction: a case study of the Triassic lacustrine Zhangjiatan oil shale, southern Ordos basin, China. *Acta Geochim.*, 37(1), 134–150.

Eno Belinga, S. M. (1966). *Contribution à l'étude géologique, minéralogique et géochimique des formations bauxitiques de l'Adamaoua (Cameroun)*. PhD thesis, Université de Paris VI. 155 p.

Eno Belinga, S. M. (1972). *L'altération des roches basaltiques et le processus de bauxitisation dans l'Adamaoua (Cameroun)*. PhD thesis, Université de Paris VI. 571 p.

Essissima-Essissima, D. (2001). Modélisation $2D^{1/2}$de quelques anomalies gravimétriques du massif de l'Adamaoua (Nord-Cameroun) et ses environs : implications géodynamiques. Mémoire de Maîtrise, Universite de Yaoundé 1, Cameroun, 63 p.

Etemad-Saeed, N., Hosseini-Barzi, M., and Armstrong-Altrin, J. S. (2011). Petrography and geochemistry of clastic sedimentary rocks as evidence for provenance of the Lower Cambrian Lalun formation, Posht-e-badam block, central Iran. *J. African Earth Sci.*, 61, 142–159.

Eyong, J. T. (2003). *Litho-biostratigraphy of the Mamfe basin, SW province of Cameroon, W. Africa*. PhD thesis, University of Leeds, UK. 269 p.

Eyong, J. T., Ngueutchoua, G., Bessong, M., Hell, V. J., Bokanda Ekoko, E., Wignall, P., and Best, J. (2019). Sedimentologic and palaeoenvironmental evolution of the Mamfe Cretaceous basin (SW Cameroon): evidence from lithofacies analysis, tectonics and evaporite minerals suite. *J. African Earth Sci.*, 149, 19–41.

Fedo, C. M., Nesbitt, H. W., and Young, G. M. (1995). Unravelling the effects of potassium metasomatism in sedimentary rocks and paleosols, with implications for paleoweathering conditions and provenance. *Geology*, 23, 921–924.

Freidman, G. M. and Sanders, F. E. (1978). *Principles of Sedimentology*. Wiley, New York. 792 pages.

Fu, X. G., Wang, J., Zeng, Y. H., Tan, F. W., and He, J. L. (2011). Geochemistry and origin of rare earth elements (REEs) in the Shengli river oil shale, northern Tibet, China. *Chem. Erde*, 71, 21–30.

Gladstone, C., McClelland, H. L. O., Woodcock, N. H., Pritchard, D., and Hunt, J. E. (2018). The formation of convolute lamination in mud-rich turbidites. *Sedimentology*, 65, 1800–1825.

Guadagnin, F., Junior, F. C., Magalhaes, A. J. C., Alessandretti, L., Ballico, M. B., and Jelinek, A. R. (2015). Sedimentary petrology and detrital zircon U–Pb and Lu–Hf constraints of mesoproterozoic intracratonic sequences in the Espinhaço supergroup: implications for the Archean and Proterozoic evolution of the São Francisco Craton. *Precambrian Res.*, 266, 227–245.

Guiraudie, C. (1955). Notice explicative sur la feuille de Ngaoundéré Ouest. Carte géologique de reconnaissance à l'échelle 1/500 000. 23 p.

Hayashi, K. I., Fujisawa, H., Holland, H. D., and Ohmoto, H. (1997). Geochemistry of 1.9 Ga sedimentary rocks from northeastern Labrador, Canada. *Geochem. Cosmochim. Acta*, 61, 4115–4137.

Herron, M. M. (1988). Geochemical classification of terrigenous sands and shales from core or log data. *J. Sediment. Petrol.*, 58, 820–829.

Hoyle, J., Elderfiel, D. H., Gledhil, L. A., and Greave, S. M. (1984). The behaviour of the rare earth elements during mixing of river and sea waters. *Geochem. Cosmochim. Acta*, 48, 143–149.

Jones, B. and Manning, D. A. C. (1994). Comparison of geochemical indices used for the interpretation of palaeoredox conditions in ancient mudstones. *Chem. Geol.*, 111, 111–129.

Kande Houetchak, L. (2008). *Etude géophysique de la structure de la croûte le long du fossé tectonique de la Mbere (Sud-Cameroun)*. PhD thesis, Université Yaoundé 1, Cameroun.

Kröner, A. and Stern, R. J. (2004). *Pan-African Orogeny*, volume 1. Elsevier, Amsterdam. pp. 259–270.

Kroonenberg, S. B. (1994). Effects of provenance, sorting and weathering on the geochemistry of fluvial sand from different tectonic and climatic environment. In *Proc. 29th Int. Geol. Congr. Part A*, pages 69–81.

Lasserre, M. (1962). Notice explicative sur les feuilles de Ngaoundéré Est et Bossagoa. Partie Cameroun, Cameroun, 50p.

Le Maréchal, A. and Vincent, P. M. (1971). Le fossé crétacé du sud-Adamaoua (Cameroun). - Cahiers de ORSTOM. *Sér. Géol.*, 1, 67–83.

Liu, R., Liu, Z. J., Sun, P. C., Xu, Y. B., Liu, D. Q., Yang, X. H., and Zhang, C. (2015). Geochemistry of the Eocene Jijuntun Formation oil shale in the Fushun basin, northeast China: implications for source-area weathering, provenance and tectonic setting. *Chem. Erde*, 75, 105–116.

Ma, P. F., Wang, L. C., Wang, C. S., Wu, X. H., and Wei, Y. S. (2015). Organic matter accumulation of the lacustrine Lunpola oil shale, central Tibetan plateau: controlled by the paleoclimate, provenance, and drainage system. *Int. J. Coal Geol.*, 147–148, 58–70.

McDonough, W. F. and Sun, S. S. (1995). The composition of the Earth. *Chem. Geol.*, 120, 223–253.

McLennan, S. M. (2001). Relationships between the trace element compositions of sedimentary rocks and upper continental crust. *Geochem. Geophys. Geosyst.*, 2, 86–98.

McLennan, S. M., Hemming, S., McDaniel, D. K., and Hanson, G. N. (1993). Geochemical approaches to sedimentation, provenance and tectonics. *Geol. Soc. Am., Spec. Pap.*, 284, 21–40.

Meng, Q. T., Liu, Z. J., Bruch, A. A., Liu, R., and Hu, F. (2012). Palaeoclimatic evolution during the Eocene and its influence on oil shale mineralisation, Fushun basin, China. *J. Asia Earth Sci.*, 45, 95–105.

Meunier, A., Caner, L., Hubert, F., El Albani, A., and Prêt, D. (2013). The weathering intensity scale (WIS): an alternative approach of chemical index of alteration (CIA). *Am. J. Sci.*, 313, 113–143.

Mongelli, G. (2004). Rare-earth elements in oligo-miocenic pelitic sediments from Lagonegro basin, southern Apennines, Italy: implications for provenance and source-area weathering. *Int. J. Earth Sci.*, 93, 612–620.

Mongelli, G., Critelli, S., Perri, F., Sonnino, M., and Perrone, V. (2006). Sedimentary recycling, provenance and paleoweathering from chemistry and mineralogy of mesozoic continental redbeb mudrocks, Peloritani mountains, southern Italy. *Geochem. J.*, 40, 197–209.

Moradi, A. V., Sarı, A., and Akkaya, P. (2016). Geochemistry of the Miocene oil shale (Hançili formation) in the Çankırı–Çorum basin, central Turkey: implications for paleoclimate conditions, source-area weathering, provenance and tectonic setting. *Sed. Geol.*, 341, 289–303.

Nagarajan, R., Armstrong-Altrin, J. S., Kessler, F. L., Hidalgo-Moral, E. L., Dodge-Wan, D., and Taib, N. I. (2015). Provenance and tectonic setting of miocene siliciclastic sediments, Sibuti formation, northwestern Borneo. *Arab. J. Geosci.*, 8, 8549–8565.

Nagarajan, R., Madhavaraju, J., Nagendra, R., Armstrong-Altrin, J. S., and Moutte, J. (2007). Geochemistry of neoproterozoic shales of Rabanpalli formation, Bhima basin, northern Karnataka, southern India: implications for provenance and Pa-leo-Redox conditions. *Rev. Mex. de Cienc. Geol.*, 24, 150–160.

Ndjeng, E. (1978). *Étude sédimentologique des niveaux à galets et à sables au Sud de l'Adamaoua (Cameroun)*. PhD thesis, Université de Dijon, France. 115 p.

Ndjeng, E. (1992). Etudes de la sédimentation et du modèle d'évolution géodynamique de deux bassins du Crétacé inférieur du Nord-Cameroun : Babouri–Figuil et Mayo Oulo-Léré. Thèse d'Etat, Université de Yaoundé, 311 p.

Ndjeng, E. and Brunet, M. (1998). Deux appareils datés de l'Hauterivien–Barremien dans le Nord-Cameroun (Fossé de la Bénoué): Les bassins de Babouri–Figuil et du Mayo Oulo-Léré. *Ann. Fac. Sci.*, 3, 97–106.

Nesbitt, H. W. and Young, G. M. (1982). Early proterozoic climates and plate motions inferred from ma-

jor element chemistry of lutites. *Nature*, 299, 715–717.

Nesbitt, H. W. and Young, G. M. (1984). Prediction of some weathering trends of plutonic and volcanic rocks based on thermodynamic and kinetic consideration. *Geochem. Cosmochim. Acta*, 48, 1523–1534.

Ngangom, E. (1983). Etude tectonique du fossé crétacé de la Mbéré et du Djerem, Sud-Adamaoua, Cameroun. *Bull. Cent. Rech. Explor. Prod. Elf Aquitaine*, 7(1), 339–347.

Ngueutchoua, G., Ekoa Bessa, A. Z., Eyong Taken, J., Demanou Zandjiob, D., Djaoroa Baba, H., and Tchami Nfada, L. (2019). Geochemistry of Cretaceous fine-grained siliciclastic rocks from upper Mundeck and Logbadjeck formations, Douala sub-basin, SW Cameroon: implications for weathering intensity, provenance, paleoclimate, redox-condition, and tectonic setting. *J. African Earth Sci.*, 152, 215–236.

Ngueutchoua, G., Ngantchu, L. D., Youbi, M., Ngos III, S., Beyala, V. K. K., Yifomju, K. P., and Tchamgoué, J. C. (2017). Geochemistry of Cretaceous mudrocks and sandstones from Douala sub-basin, Kumba area, south west Cameroon: constraints on provenance, source rock weathering, paleo-oxidation conditions and tectonic environment. *Int. J. Geosci.*, 8, 393–424.

Njoh, O. A., Nforsi, M. B., and Datcheu, J. N. (2015). Aptian-late Cenomanian fluvio-lacustrine lithofacies and palynomorphs from Mamfe basin, southwest Cameroon, West Africa. *Int. J. Geosci.*, 6, 795–811.

Nothdurft, L. D., Webb, G. E., and Kamber, B. S. (2004). Rare earth element geochemistry of late Devonian reefal carbonates, Canning basin, Western Australia: confirmation of a seawater REE proxy in ancient limestones. *Geochem. Cosmochim. Acta*, 68(2), 263–283.

Noutchogwe Tatchum, C. (2004). *Apport de la gravimétrie a l'étude de la bordure méridionale du plateau de l'Adamaoua (Cameroun)*. PhD thesis, Univ. Yaoundé 1, Cameroun.

Noutchogwe Tatchum, C., Koumetio, F., and Manguelle-Dicoum, E. (2010). Traits structuraux du Sud-Adamaoua (Cameroun) déduits des anomalies magnétiques: implications hydrogéologiques. *C. R. Géosci.*, 342, 467–474.

Nozaki, Y., Zhang, J., and Amakawa, H. (1997). The fractionation between Y and Ho in the marine environment. *Earth Planet. Sci. Lett.*, 148, 329–340.

Nzenti, J. P., Barbey, P., Macaudière, J., and Soba, D. (1988). Origin and evolution of the late Precambrian high grade Yaounde gneisses (Cameroon). *Precambrian Res.*, 38, 91–109.

Penaye, J., Toteu, S. F., Michard, A., Van Schmus, W. R., and Nzenti, J. P. (1993). U–Pb and Sm–Nd preliminary geochronologic data on the Yaoundé series, Cameroon: reinterpretation of granulitic rock as the suture of the collision in the "Centrafricain" belt. *C. R. Acad. Sci. Paris*, 317, 789–794.

Perri, F. (2014). Composition, provenance and source weathering of mesozoic sandstones from western-central mediterranean Alpine chains. *J. African Earth Sci.*, 91, 32–43.

Perri, F., Critelli, S., Mongelli, G., and Cullers, R. L. (2011). Sedimentary evolution of the mesozoic continental redbeds using geochemical and mineralogical tools: the case of upper triasic to lowermost Jurassic Monte di Gioiosa Mudrocks (Sicily, southern Italy). *Int. J. Earth Sci.*, 100, 1569–1587.

Rashid, S. A., Gana, I. J. A., Masoodi, A., and Khan, F. A. (2015). Major and trace element geochemistry of lake sediments, India: implications for weathering and climate control. *Arab. J. Geosci.*, 8, 10481–10496.

Ravier, J. (1959). *Le métamorphisme des terrains secondaires des Pyrénées*. Mém. Soc. Géol., France.

Reineck, H. E. and Singh, I. B. (1980). *Depositional Sedimentary Environments*. Springer-Verlag, New York.

Rimmer, S. M. (2004). Geochemical Paleoredox indicators in Devonian–Mississippian black shales, central Appalachian basin (USA). *Chem. Geol.*, 206, 373–391.

Roser, B. P., Cooper, R. A., Nathan, S. A., and Tulloch, A. J. (1996). Reconnaissance sandstone geochemistry, provenance, and tectonic setting of the lower Paleozoic terrains of the west coast and Nelson, New Zealand. *New Zealand J. Geol. Geophys.*, 39, 1–16.

Ross, D. J. K. and Bustin, R. M. (2009). Investigating the use of sedimentary geochemical proxies for paleoenvironment interpretation of thermally mature organic-rich strata: examples from the Devonian–Mississippian shales, western Canadian sedimentary basin. *Chem. Geol.*, 260, 1–19.

Shi, Z. S., Chen, K. Y., Shi, J., Liu, B. J., He, H. J., and

Liu, G. (1994). Feasibility analysis of the application of the ratio of strontium to barium on the identifying sedimentary environment. *Fault-Block Oil Gas Field*, 10, 12–16.

Suttner, L. and Dutta, P. (1986). Alluvial sandstone composition and paleoclimate, I. Framework mineralogy. *J. Sediment. Petrol. A*, 56(3), 329–345.

Tao, H., Wang, Q., Yang, X., and Jiang, L. (2013). Provenance and tectonic setting of late Carboniferous clastic rocks in west Junggar, Xinjiang, China: a case from the Hala-alat mountains. *J. Asian Earth Sci.*, 64, 210–222.

Tawfik, H. A., Salah, M. K., Maejima, W., Armstrong-Altrin, J. S., Abdel-Hameed, A. M. T., and El Ghandour, M. M. (2017). Petrography and geochemistry of the Lower Miocene Moghra sandstones, Qattara depression, north Western Desert, Egypt. *Geol. J.*, pages 1–16.

Taylor, S. R. and McLennan, S. M. (1985). *The Continental Crust: Its Composition and Evolution*. Blackwell Scientific, Oxford.

Tchouatcha, M. S. (2011). *Les bassins du Mbere et du Djerem dans le contexte régional Sud Adamaoua: genèse, évolution stratigraphique et reconstitution des paléoenvironnements*. PhD thesis, Université de Yaoundé 1, Cameroun. 225 p.

Tchouatcha, M. S., Njike Ngaha, P. R., Mahmoud, M. S., Deaf, A. S., and Ekodeck, G. E. (2010). Existence of "late continental" deposits in the Mbere and Djerem sedimentary basins (north Cameroon): palynologic and stratigraphic evidence. *J. Geol. Min. Res.*, 2(6), 159–169.

Tchouatcha, M. S., Njoya, A., Ganno, S., Toyama, R., Ngouem, P. A., and Njike Ngaha, P. R. (2016). Origin and paleoenvironment of Pleistocene–Holocene Travertine deposit from the Mbere sedimentary sub-basin along the central Cameroon shear zone: insights from petrology and palynology and evidence for neotectonics. *J. African Earth Sci.*, 118, 24–34.

Teng, G. E., Hui, L. W., Xu, Y. C., and Chen, J. F. (2005). Correlative study on parameters of inorganic geochemistry and hydrocarbon source rocks formative environment. *Adv. Earth Sci.*, 20(2), 193–200.

Toteu, F. S., Penaye, J., and Poudjom Djomani, Y. (2004). Geodynamic evolution of the Pan-African belt in central Africa with special reference to Cameroon. *Can. J. Earth Sci.*, 41, 73–85.

Tribovillard, N., Algeo, T. J., Lyons, T., and Riboulleau, A. (2006). Trace metals as paleoredox and paleoproductivity proxies an update. *Chem. Geol.*, 232(1–2), 12–32.

Verma, S. P. and Armstrong-Altrin, J. S. (2013). New multi-dimensional diagrams for tectonic discrimination of siliciclastic sediments and their application to Precambrian basins. *Chem. Geol.*, 355, 117–133.

Wang, M. F., Jiao, Y. Q., Wang, Z. H., Yang, Q., and Yang, S. K. (2005). Recovery paleo-salinity in sedimentary environment: an example of mudstone in Shuixigou group, southwestern margin of Turpan-Hami basin, Xin Jiang. *Petrol. Geol.*, 12, 719–722.

Wen, H., Zheng, R., Geng, W., Fan, M., and Wang, M. (2007). Characteristics of rare earth elements of lacustrine exhalative rock in the Xiagou formation of lower Cretaceous in Qingxi sag. Jiuxi basin. *Front. Earth Sci. China*, 1(3), 333–340.

White, A. F. and Blum, A. E. (1995). Effects of climate on chemical weathering in watersheds. *Geochem. Cosmochim. Acta*, 59, 1729–1747.

Xie, G., Shen, Y., Liu, S., and Hao, W. (2018). Trace and rare earth element (REE) characteristics of mudstones from Eocene Pinghu formation and Oligocene Huagang formation in XihuSag, east China sea basin: implications for provenance, depositional conditions and paleoclimate. *Mar. Petrol. Geol.*, 1, 1–35.

Xu, B. H., Ding, S. L., Wang, Y., and Liu, Q. F. (2011). Geochemical characteristics of illite clay rocks from the Shihezi formation in the Hanxing mining area and its sedimentary environment. *Mining Sci. Tech. (China)*, 21, 495–500.

Yan, D. T., Chen, D. Z., Wang, Q. C., and Wang, J. G. (2010). Large-scale climate fluctuations in the latest Ordovician on the Yangtze block, south China. *Geology*, 38, 599–602.

Zaid, S. M. (2015). Geochemistry of sands along the Ain Soukhna and Ras Gharib beaches, Gulf of Suez, Egypt: implications for provenance and tectonic setting. *Arab. J. Geosci.*, 8, 10481–10496.

Zeng, S., Wang, J., Chen, W., Fu, X., Feng, X., Song, C., Wang, D., and Sun, W. (2019). Geochemical characteristics of early Cretaceous marine oil shale from Changshe Mountain area in the northern Qiangtang Basin, Tibet: implication for palaeoweathering, provenance, tectonic setting, and organic matter accumulation. *Geol. J.*, pages 1–18.

Zhao, B. S., Jin, Z., Geng, Y., Wen, X., and Yan, C.

(2016). Applying sedimentary geochemical proxies for paleoenvironment interpretation of organic-rich shale deposition in the Sichuan basin, China. *Int. J. Coal Geol.*, 163, 52–71.

Zheng, R. C. and Liu, M. Q. (1999). Study on palaeosalinity of Chang-6 oil reservoir set in Ordos basin. *Oil Gas Geol.*, 20, 20–25.

Zou, S., Wu, C., Xu, D., Shan, Q., Zhang, X., and Hollings, P. (2016). Provenance and depositional setting of lower Silurian siliciclastic rocks on Hainan Island, south China: implications for a passive margin environment of south China in Gondwana. *J. Asian Earth Sci.*, 123, 243–262.